

Article

Differences in Spatiotemporal Variability of Potential and Reference Crop Evapotranspirations

Keyu Xiang^{1,2,†}, Xuan Zhang^{3,†}, Xiaofeng Peng³, Ning Yao^{2,4} , Asim Biswas⁵ , Deli Liu⁶ , Yufeng Zou², Bakhtiyor Pulatov⁷, Yi Li^{2,3,4,*} and Fenggui Liu^{8,*}

- ¹ College of Water Resources and Architectural Engineering, Shihezi University, Shihezi 832003, China; xiangkiris@nwafu.edu.cn
 - ² College of Water Resources and Architectural Engineering, Northwest Agriculture and Forestry University, Xianyang 712100, China; yaoning@nwafu.edu.cn (N.Y.); matthew1222@163.com (Y.Z.)
 - ³ Institute of Agricultural Science of the Third Division of Xinjiang Production and Construction Corps, Tumushuke 843900, China; zhangx@126.com (X.Z.); pengxf2016@163.com (X.P.)
 - ⁴ Key Laboratory for Agricultural Soil and Water Engineering in Arid Area of Ministry of Education, Northwest A&F University, Xianyang 712100, China
 - ⁵ School of Environmental Sciences, University of Guelph, Guelph, ON N1G 2W1, Canada; biswas@uoguelph.ca
 - ⁶ NSW Department of Primary Industries, Wagga Wagga Agricultural Institute, Wagga Wagga, NSW 2650, Australia; de.li.liu@dpi.nsw.gov.au
 - ⁷ Tashkent Institute of Irrigation and Agricultural Mechanization Engineers—National Research University, Qoriy Niyoziy 39, Tashkent 100000, Uzbekistan; bakhtiyor.pulatoff@gmail.com
 - ⁸ Academy of Plateau Science and Sustainability, Qinghai Normal University, Xining 810008, China
- * Correspondence: liyikitty@126.com (Y.L.); lfg_918@163.com (F.L.)
† These authors contributed equally to this work.



Citation: Xiang, K.; Zhang, X.; Peng, X.; Yao, N.; Biswas, A.; Liu, D.; Zou, Y.; Pulatov, B.; Li, Y.; Liu, F. Differences in Spatiotemporal Variability of Potential and Reference Crop Evapotranspirations. *Water* **2022**, *14*, 988. <https://doi.org/10.3390/w14060988>

Academic Editor: Renato Morbidelli

Received: 9 February 2022

Accepted: 17 March 2022

Published: 21 March 2022

Publisher's Note: MDPI stays neutral with regard to jurisdictional claims in published maps and institutional affiliations.



Copyright: © 2022 by the authors. Licensee MDPI, Basel, Switzerland. This article is an open access article distributed under the terms and conditions of the Creative Commons Attribution (CC BY) license (<https://creativecommons.org/licenses/by/4.0/>).

Abstract: Potential evapotranspiration (ET_p) and reference crop evapotranspiration (ET_o) are two key parameters in hydrology, meteorology, and agronomy. ET_p and ET_o are related to each other but have different meanings and applications. In this study, the ET_p and ET_o were distinguished and calculated with the Penman and FAO56 PM equations using the weather data of 551 stations in China from 1961 to 2018. The differences in their spatiotemporal variations were examined with an MMK test, an R/S test, and wavelet analysis. The monthly ET_p and ET_o were close but the ET_p was always larger than the ET_o , with values ranging from 1 to 356 mm and 2 to 323 mm, respectively. Their differences varied in different months and sub-regions. The maximum monthly difference transferred from south to north and then back to the south in a yearly cycle, showing spatiotemporal heterogeneity. The annual values of the ET_p and ET_o were also close, but the ET_p was significantly higher than the ET_o . The increasing future trends of ET_p but decreasing trends of ET_o were tested at most sites in China. Although the primary periods were almost the same, their spatial distribution was slightly different. In conclusion, ET_p is different from ET_o and they should be applied carefully. This study performs a thorough comparison and reveals the underlying basis of and discrepancy between ET_p and ET_o .

Keywords: potential evapotranspiration; reference crop evapotranspiration; R/S analysis; wavelet analysis; spatiotemporal variability

1. Introduction

Potential evapotranspiration (ET_p) and reference crop evapotranspiration (ET_o) are closely connected to actual evapotranspiration (ET) [1,2], leading them to be extensively used in the fields of hydrology, agronomy, meteorology, and ecology [1–5]. Moreover, an important practical application of ET in the fields mentioned above is crop evapotranspiration (ET_c) [6], which is usually calculated by ET_p or ET_o to evaluate the regional or global variation in agricultural water quantity [7,8], to assess the impacts or responses to

climate change [9–11], and to provide useful guidelines for related policy makers. The accuracy estimation of ET_p or ET_o is key for achieving these aims. Therefore, the difference between ET_p and ET_o needs further analysis. Many recent research involving ET_p or ET_o has focused on their variation, regional characteristics [12] or prediction [13], drought or drying analysis [14], vegetation responses [15], responses to drought [16], the influence of water resources on agriculture [17], and evapotranspiration rate estimations [18]. The studied timescales varied from monthly to annual [2,19], and the spatial scales varied from site [20] to multi-site [19], regional [21], national, and global. Additionally, many interesting results were obtained, the calculation efficiency was improved, and a software was created [22].

The development of definitions for ET_p and ET_o has been a long-term process. Thornthwaite (1948) defined ET_p as “the maximal water vapor in an area, including the evapotranspiration from crops and the evaporation from water surfaces in order to determine dry/wet conditions” [23]. Although other definitions have been suggested [24–29], the definition of ET_p has not yet been standardized. Doorenbos and Pruitt (1977) proposed a clear concept of ET_o [30]. The Food and Agriculture Organization (FAO) standardized the ET_o definition as “the ratio of evapotranspiration from a reference crop with an assumed crop height of 12 cm, a fixed surface resistance at 70 s/m, and albedo of 0.23 which closely resembles evapotranspiration from an extensive surface of green grass cover without water stress” [6].

Despite some similarities, there are many differences between ET_p and ET_o in terms of their definition, estimation methods, equation types, and application fields. Much of the previous research has mixed the utilization of these two terms. Instances of this misuse are as follows. (i) Use of incorrect terminology [31–33]: For example, Sun et al. adopted the FAO 56 Penman–Monteith equation to estimate ET_o , but they named it “potential evapotranspiration” [34,35]. (ii) The alternative and inconsistent use of the two terms (Gwate et al., 2018; Lewis and Allen 2017; Zhang 2019) [5,36,37]: When Ding et al. (2020) adopted the FAO 56 Penman–Monteith equation to estimate ET_o in northwest China, they used both terms—“potential evapotranspiration” and “reference evapotranspiration” [38]. (iii) The application of mixed equations. For example, Oudin et al. (2005) generalized four different types of ET_p , when in fact the FAO-24 and Hargreaves and Samani (1982) were ET_o equations. Burke et al. (2006) adopted an ET_o equation to estimate ET_p when conducting a drought analysis [30,39–42].

Except for some common misuses, most researchers have used ET_o [6,43–49] or ET_p correctly [50–52]. However, their attributions have rarely been compared. For example, Katerji and Rana (2011) investigated the differences between ET_p and ET_o by comparing resistances (namely, the aerodynamic resistance, crop-structure resistance and crop-stomatal resistance) [53]. They concluded that ET_o and ET_p were un-equivalent. Xiang et al. (2020) reviewed the differences between the two terms and grouped the different types of ET_p and ET_o [54]. This was the first study to clearly differentiate ET_p and ET_o up until now.

Many researchers consider ET_p and ET_o to be equivalent. Due to the difficulty in their direct and accurate measurement, the differences in these closely related terms when supporting and modelling results are often considered to be errors or uncertainties, even though these can be reduced through the proper choice of the type of ET . Accuracy estimations of ET_p and ET_o affect both the water-resource and agricultural sectors and contributes significantly to the national economy [50]. Although there has been progress in differentiating ET_p and ET_o , a direct quantitative comparison between them is missing, despite their contributions to the fields of agriculture, engineering, and the environment. Thus, this research aims to quantitatively compare ET_p and ET_o at monthly and annual timescales for mainland China based on their commonly used and standardized methods. The spatiotemporal variability characteristics, including trends, abrupt-change years, the wavelet-based main- and quasi-periods, and the serial long-term dependence, will be systematically compared. This work will provide important references for researchers in a wide range of fields who directly or indirectly use potential or reference crop evapotranspiration.

2. Data Collection and Methodology

2.1. Study Area Description and Data Sources

China is located in eastern Eurasia on the west coast of the Pacific Ocean. It has a large land mass ($9.634057 \times 10^6 \text{ km}^2$); a long distance between its eastern and western boundaries; a wide range of altitudes, morphologies, and mountains; and a variety of climates. Weather data from 839 stations of China were downloaded from the Meteorological Data Sharing Service Network in China (<http://data.cma.cn/>, accessed on 6 March 2017). The daily climatic variables include precipitation, wind speed at 10 m (u_{10}), the maximum (T_{\max}) and minimum air temperature (T_{\min}), relative humidity, and hours of sunshine, from December 1960 to December 2018. The sites with a data-missing ratio $>1\%$ were removed. Missing data were interpolated with the data of 10 adjacent sites on the same day. The data were cross-examined using the Kendall autocorrelation and Mann–Whitney homogeneity tests [55]. The test results indicated that the fluctuation of the weather data was fixed between critical points at a significance level of 5% [56,57]. Finally, a total of 551 sites were selected.

The digital elevation and the site distribution in mainland China are presented in Figure 1. There are seven climate zones, including the northwestern desert region, the Inner Mongolia grassland region, the Qinghai–Tibetan Plateau, the northeastern humid and sub-humid region, the northern China humid and semi-humid region, the middle and southern China humid and sub-tropical region, and the southern China humid and tropical region, which are named as sub-regions I to VII and which contain 46, 47, 39, 69, 108, 190, and 52 weather stations, respectively. Sub-region III contains fewer stations due to its relatively rough terrain with high elevation range. The analysis will consider both mainland China and these divided sub-regions.

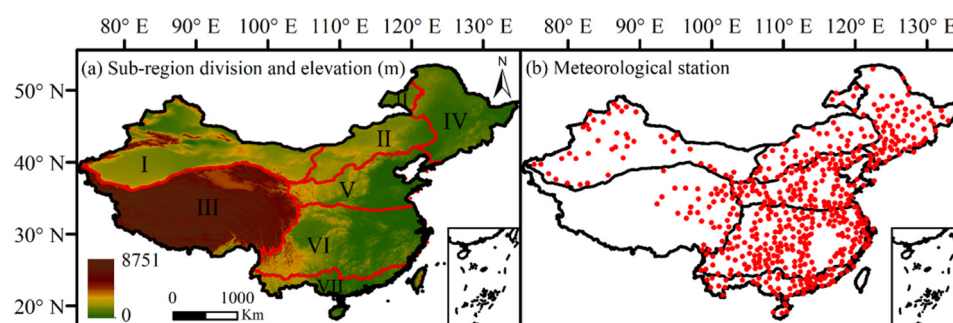


Figure 1. The digital evaluation of the sub-region divisions and the distribution of the weather stations. (a) Sub-region division and elevation; (b) Meteorological station.

2.2. Methodology

2.2.1. Equations for Estimating ET_p and ET_o

The Penman (1963) equation was selected as the standardized ET_p method, since this formula was developed from the Penman (1948) equation and is one of the earliest methods used to calculate ET_p [25]. It is a widely used equation [58–60], written as [25]:

$$ET_p = \frac{\Delta}{\Delta + \gamma} (R_n - G) + \frac{6.43\gamma}{\Delta + \gamma} (1 + 0.0536u_2)(e_s - e_a) \quad (1)$$

where Δ is the slope of the vapor–pressure curve ($\text{kPa } ^\circ\text{C}^{-1}$); γ is the psychrometric constant ($\text{kPa } ^\circ\text{C}^{-1}$); u_2 and T_2 are the wind speed (m s^{-1}) and mean air temperature ($^\circ\text{C}$) at 2 m; e_s and e_a are the saturation and actual vapor pressure (kPa), respectively (kPa); R_n is the net radiation ($\text{MJ m}^{-2} \text{ day}^{-1}$); and G is the soil heat flux ($\text{MJ m}^{-2} \text{ day}^{-1}$). Values of u_2 are obtained based on u_{10} . G at the M th month is estimated by the soil temperature of $M+1$ th and $M-1$ th month:

$$G_M = 0.07 (T_{M+1} - T_{M-1}) \quad (2)$$

The standardized ET_o method of the Penman–Monteith equation is written as [6]:

$$ET_o = \frac{0.408\Delta(R_n - G) + \gamma u_2(e_s - e_a)[900 / (T_2 + 273)]}{\Delta + \gamma(1 + 0.34u_2)} \tag{3}$$

Annual ET_o or ET_p values are found by summing the monthly values.

2.2.2. Trend and Abrupt-Change Year Analysis

The trends and significance of the annual ET_o (or ET_p) series at the 551 sites were tested following the modified nonparametric Mann–Kendall (MMK) method [61]. The MMK considers the effects of self-correlation in time series $x(t)$ ($t = 1, 2, \dots, N_T$, where N_T is the total year number) based on the Mann–Kendall method [62,63]. To show the influence of serial self-correlation, the MK statistic is modified to the new MMK statistic (Z_m) with a correction factor n^s [64]. If Z_m is positive/negative, $x(t)$ has an up/downward trend. When the lag of self-correlation functions is >0 and $|Z_m| \geq 1.96$, x_i is time-dependent and the trend is significant at a confidence level $\alpha = 0.05$. The equations are written as follows:

$$Z^* = \frac{Z}{\sqrt{n_1^s}}, \text{ where } n_1^s = \begin{cases} 1 + \frac{2}{n_1} \sum_{jj=1}^{n_1-1} (n_1 - 1)r_{jj} & \text{for } jj > 1 \\ 1 + 2 \frac{r_1^{n_1+1} - n_1 r_1^2 + (n_1 - 1)r_1}{n_1(r_1 - 1)^2} & \text{for } jj > 1 \end{cases} \tag{4}$$

where r_{jj} is the self-correlation coefficient of the time series at the lag- jj .

2.2.3. The Rescaled (R/S) Analysis

The R/S analysis was proposed based on Hurst (1951) [65,66]. For the time series $x(t)$ ($t = 1, 2, \dots, 58$), the mean value and cumulative deviation of the sub-series are calculated as:

$$y(\tau) = \frac{1}{\tau} \sum_{t=1}^{\tau} x(t), \tau = 1, 2, \dots \tag{5}$$

$$F(t, \tau) = \sum_{u=1}^{\tau} x(u) - y(\tau), 1 \leq t \leq \tau \tag{6}$$

The range is calculated as:

$$R(\tau) = \max_{1 \leq t \leq \tau} F(t, \tau) - \min_{1 \leq t \leq \tau} F(t, \tau), F(t, \tau) = 1, 2, \dots \tag{7}$$

Additionally the standardized deviation is computed as:

$$S(\tau) = \left[\frac{1}{\tau} \sum_{t=1}^{\tau} (x(t) - y(\tau))^2 \right]^{\frac{1}{2}}, \tau = 1, 2, \dots \tag{8}$$

The ratio of the range to standardized deviation is described as:

$$\frac{R(\tau)}{S(\tau)} = (C\tau)^H, \text{ then } \log(R/S)n = \log C + H \log n \tag{9}$$

where C is a constant. By applying Equation (11), the Hurst index ($0 < H < 1$) is obtained. H measures the intensity of long-range dependence in $x(t)$. When $H = 0.5$, the time series $x(t)$ has a random process. When $0 < H < 0.5$ and $0.5 < H < 1$, $x(t)$ has reversibility or sustainability, respectively.

2.2.4. The Wavelet Analysis

A continuous wavelet transform was performed using the Morlet wavelet basis (Ψ_0) [67]. The wavelet key function is described as:

$$\int_{-\infty}^{+\infty} \Psi(t)dt = 0 \tag{10}$$

where t is the year and $\Psi(t)$ is a wavelet function that can form a cluster of functions on the timeline (Li et al., 2019):

$$\Psi_{a,b}(t) = |a|^{-\frac{1}{2}} \Psi\left(\frac{t-b}{a}\right), a, b \in R, a \neq 0 \tag{11}$$

where $\Psi_{a,b}(t)$ is a sub-wavelet, a is a wavelet-length scale factor, and b is a factor that shows the translation in time. The multi-Morlet-wavelet was selected as a basic function here.

The primary period has a maximum vibration intensity showing the significance or insignificance which is read from the bright color-belt of the wavelet map. The quasi-period has a secondary maximum vibration intensity [68]. The MATLAB 2019b software (MathWorks, Natick, MA, USA) was used to perform these analyses.

A schematic of general framework adopted in this research is presented in Figure 2.

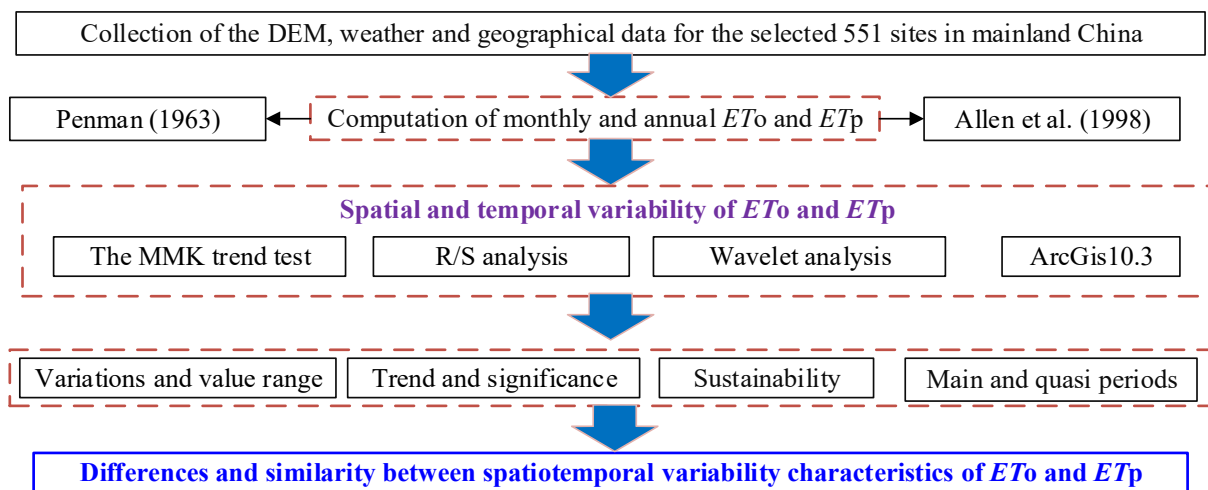


Figure 2. Flow chart of the study framework used for this research.

3. Results

3.1. The Differences between Monthly ET_p and ET_o

3.1.1. Temporal Differences

The temporal variations in the monthly ET_p and ET_o between 1961 and 2018 averaged from 551 sites across China are presented in Figure 3. The monthly ET_p and ET_o fluctuated periodically and their peaks and valleys varied synchronically. The monthly ET_p were larger than the monthly ET_o between 1961 and 2018. The monthly ET_p and ET_o differed clearly in their values.

To further show the value differences, the scatter plots of ET_p and ET_o between 1961 and 2018 in the 12 months of the year are shown in Figure 4. The monthly ET_p and ET_o ranged from 1 to 356 mm and from 2 to 323 mm, respectively. Most of the data-points were in the upper-left side of the 1:1 line, and some large values were in the upper-right part of the 1:1 line. These generally indicated a larger monthly ET_p than ET_o , especially in the cold months of November to March. The deviations of the monthly ET_p from ET_o were larger and increased with the increase in their values. Furthermore, the slopes of the linear function ranged between 1.11 and 1.30, indicating deviations of 11–30% from the monthly ET_p to ET_o . There were very high R^2 values (0.89–0.95) representing a linear correlation

between ET_p and ET_o , which confirmed the similarity in their patterns. Although there were slight differences in the R^2 values of the cold months and warm months, this may be due to the variation in the meteorological data, which were using different weights in the two ET equations. Across the entire study area in each month, the relationship between the two was generally close.

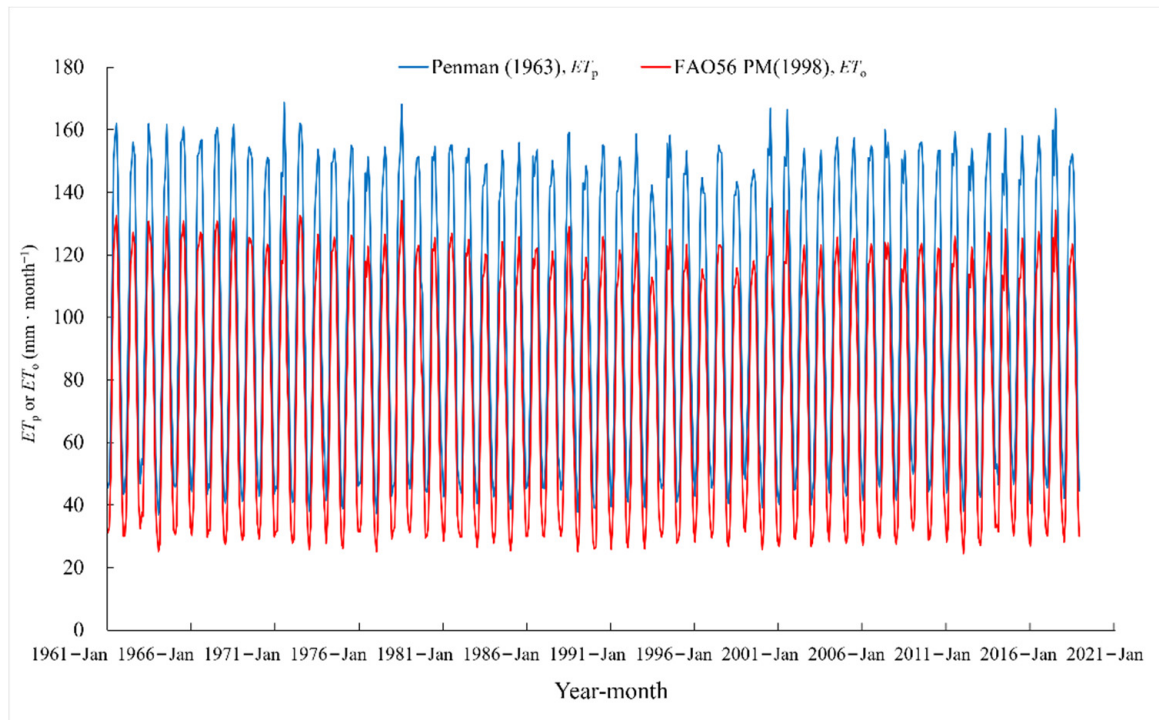


Figure 3. The variations in monthly ET_o and ET_p averaged from 551 sites in mainland China.

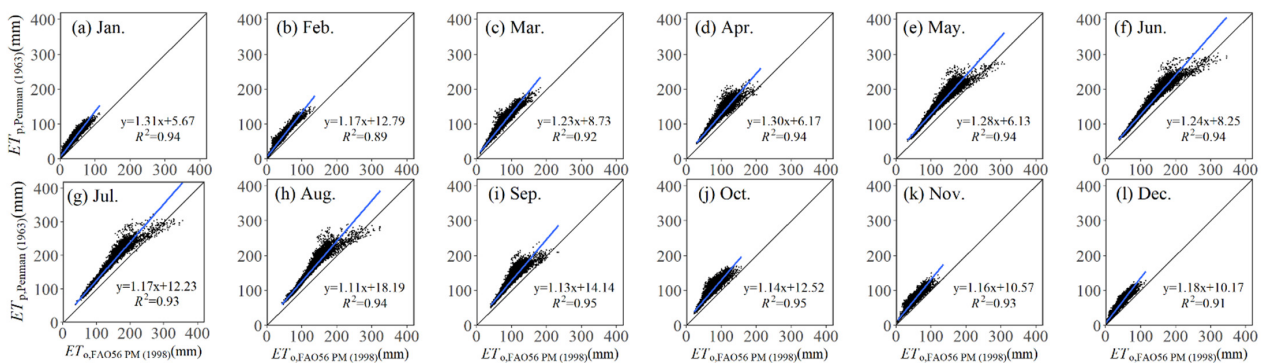


Figure 4. The scatter plots of monthly ET_o and ET_p for the 12 months (containing 551 sites).

The variations in long-term mean monthly ET_p , ET_o , and their differences $D (=ET_p - ET_o)$ were also compared for the different sub-regions (Figure 5). The monthly ET_p , ET_o , and D showed peaks from around May to July. The peak values of ET_p and ET_o ranged from 144 to 218 mm and 116 to 176 mm for the sub-regions I to VII and for Mainland China, respectively. The peaks in the sub-regions ranked in the order of $I > II > V > \text{Mainland China} > IV > VII > VI > III$. The interannual variations in ET_p and ET_o were larger for the arid and semi-arid sub-regions (I and II) than the semi-humid and humid sub-regions (III, VI and VII). The monthly ET_p were generally larger than the monthly ET_o for the same month and the same region. The D values varied within the months of the year, reaching as high as 42 mm in July for the arid and semi-arid sub-region I.

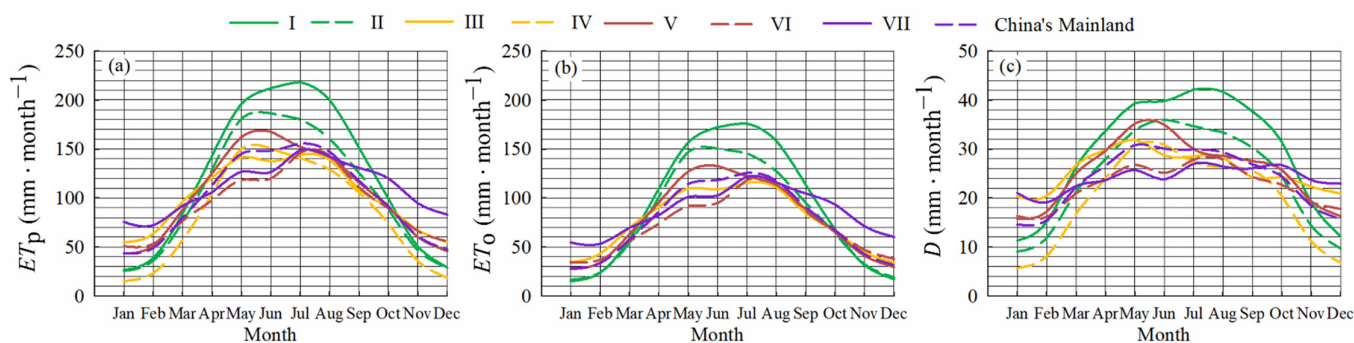


Figure 5. The long-term mean monthly variables averaged from the sites of different sub-regions. (a) ET_p , (b) ET_0 and (c) D .

Figures 3–5 show that the monthly ET_p was larger than ET_0 under most conditions. Although previous research has investigated the temporal variations in monthly ET_p or ET_0 , seldom has research directly compared their values with the aim of differentiating the two variables.

3.1.2. Spatial Differences

The spatial distribution of the long-term mean monthly $D (=ET_p - ET_0)$ in the 12 months of the year (Figure 6) exhibited variable ranges between ET_p and ET_0 across China. The results showed that: (1) The monthly D varied with the months. In cold and cool seasons (October to March), the smallest D values were in northeastern China and the areas of northwestern China. D values were mostly positive in mainland China, since the ET_p values were generally larger than the ET_0 . (2) In the warm and hot seasons (April to September), the smallest D values were observed in southeastern or northeastern China. These were mostly positive but were occasionally negative, reaching as low as -9 mm month^{-1} . The D values in sub-regions II (the Inner Mongolia grassland), III (the Qinghai-Tibetan Plateau), and V (northern China) were large. (3) In sub-region IV (northeastern China), the D values ranged between 2 and 33 mm month^{-1} in the year and did not change as much as other regions. (4) In general, the spatial distributions of the monthly D were both site- and region-specific.

The detailed differences in the D for the various sub-regions and months are presented in Table 1.

Table 1. Values of the monthly D in different sub-regions and months. Unit: mm month^{-1} .

Month	Sub-Region						
	I	II	III	IV	V	VI	VII
January	15	11	9	20	6	16	16
February	15	15	12	20	8	17	16
March	22	26	21	27	17	25	21
April	27	34	28	30	24	30	24
May	31	39	34	32	31	35	27
June	30	40	36	29	31	35	25
July	30	42	35	29	27	30	28
August	29	42	33	28	26	29	28
September	27	38	30	24	26	28	24
October	24	31	24	24	20	26	23
November	18	19	14	22	11	19	19
December	16	12	10	21	7	16	18

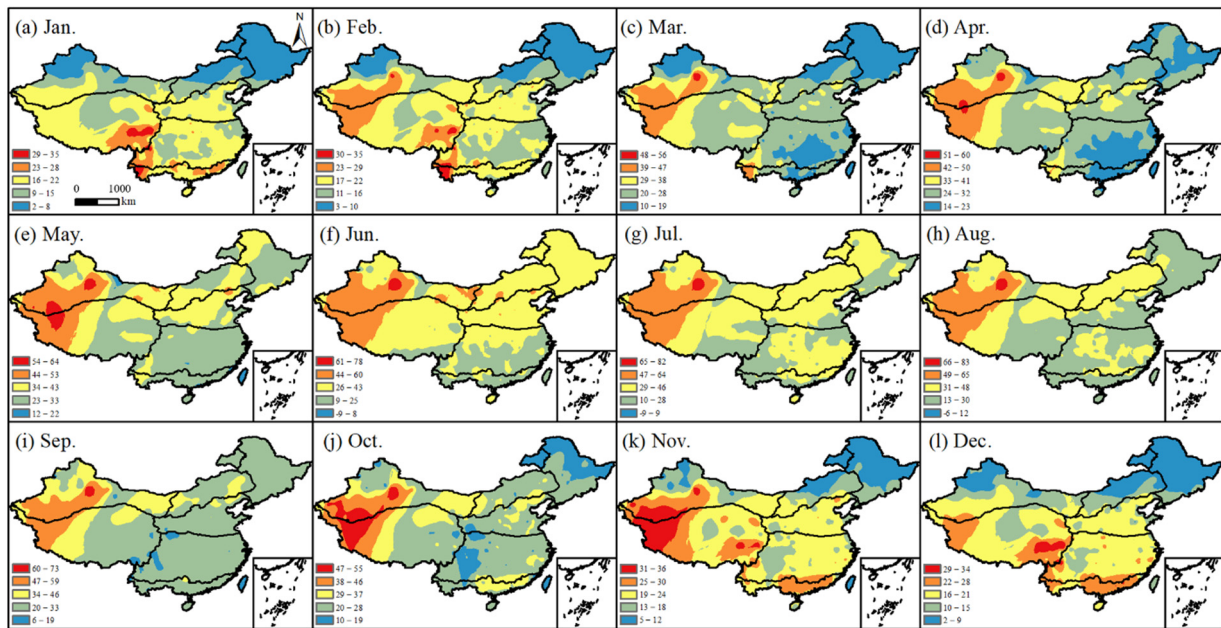


Figure 6. The spatial distribution of the long-term mean monthly D in mainland China (the site values were interpolated by the Kriging method in ArcGIS 10.3).

3.2. The Differences between Annual ET_p and ET_o

3.2.1. Temporal and Spatial Differences

The annual variations in the ET_p and ET_o in different sub-regions of China are presented in Figure 7. The fluctuating patterns of the ET_p and ET_o in the same sub-region were generally similar. The general sub-region ranks of the annual ET_p and ET_o values were sub-region I > III > II > VII > IV > V > VI > mainland China. The annual D values ranged from 256 mm to 315 mm for sub-regions I to VII and mainland China. It was observed that the annual ET_p differed with the ET_o and the differences varied within the different sub-regions.

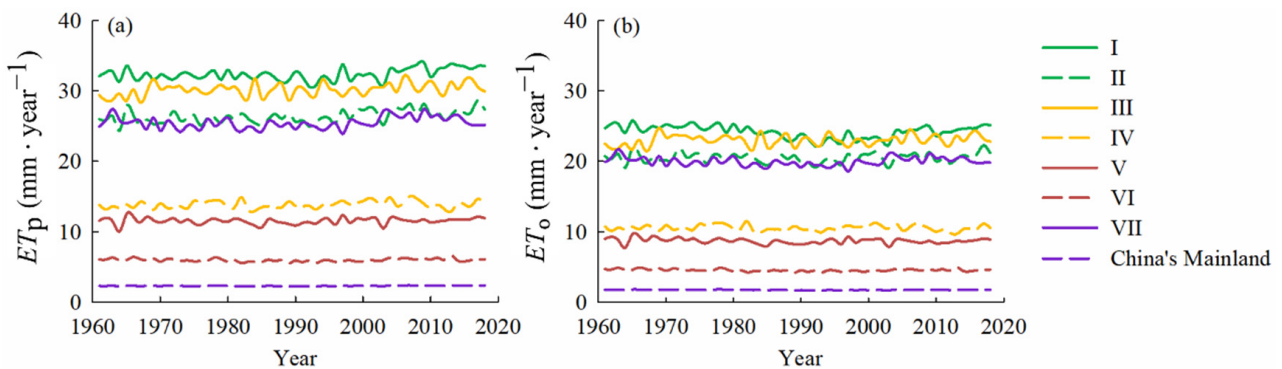


Figure 7. The temporal variations in annual variables in different sub-regions of China. The sub-regional ET_p and ET_o values were computed using the site-specific weight coefficients obtained from the Theson-polygon method in ArcGis. (a) ET_p and (b) ET_o .

The spatial distribution of the long-term mean annual ET_p , ET_o and D in mainland China are presented in Figure 8. The spatial distribution pattern of the annual ET_p and ET_o were similar; low values appeared in northeastern, central, and southern China, but large values appeared in northwestern and southern China. The ranges of the annual ET_p and ET_o differed from 778 to 1738 mm and from 585 to 1357 mm, respectively. The annual D values ranged from 36 to 681 mm and the highest values occurred in northwestern China

and northern China. Therefore, in the areas with high D values, the differences in ET_p and ET_o should be considered in case their incorrect utilization should cause deviations.

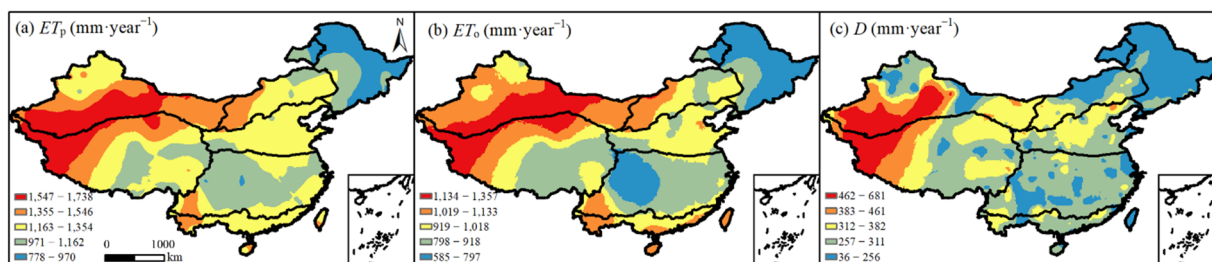


Figure 8. The spatial distribution of longterm mean annual (a) ET_p , (b) ET_o , and (c) D in mainland China.

3.2.2. The Trends and Long—Term Dependence

To further compare the intrinsic features, the annual ET_p and ET_o for all the sites were mapped (Figure 9). Although the trend distribution of the annual ET_p and ET_o looked similar—namely, with more increasing trends seen in central, northern, and small areas of southern China—more sites had decreasing trends in their annual ET_o . Their trend significance was also different.

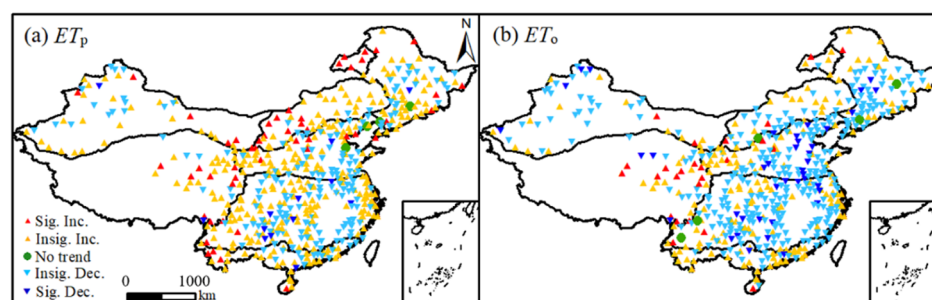


Figure 9. The trends and significance of annual ET_p and ET_o in mainland China.

The detailed numbers of the sites with different trends and significance are given in Table 2. In all the seven sub-regions, more sites had increasing trends in annual ET_p than ET_o . Thus, due to the differences in spatiotemporal distributions, the ET_p and ET_o must be used carefully and correctly in hydrology and meteorology research. Our results were different from those of Han et al. (2012), who investigated ET_p trends between 1956 and 2005 at 244 sites in China and found decreasing ET_p trends for 59.7%, 50%, and 64.2% of the total stations in the arid/semi-arid, semi-humid, and humid regions of China, respectively [51]. This was not surprising, since the studied station numbers and the studied period of the two were very different.

The spatial distributions of the Hurst index for the annual ET_p and ET_o were mapped and are presented in Figure 10. The detailed number of sites that had different ranges of the Hurst index in each sub-region are given in Table 3. The spatial distribution of the two terms were generally similar—namely, most sites had Hurst indices larger than 0.5. The sites that had different ranges of the Hurst index were also very close, but the number of ET_p for $H < 0.5$ was almost 2.5 times that of ET_o at 19 and 8 sites, respectively. This implied that the future ET_p and ET_o of most stations will maintain consistent with the previous trend, while several sites' ET_p and ET_o will probably go in the opposite direction. When the Hurst index was combined with the result of the MMK test, the ET_o trend of most sites showed an insignificant decrease, while a few sites' ET_o trend was reversed to increase in the future. In that situation, the trend of the ET_p can be derived by comparing with the ET_o .

Table 2. The station numbers of annual ET_0 and ET_p , which had different trends and levels of significance in different sub-regions.

Term	Trend	Sub-Region							Subtotal
		I	II	III	IV	V	VI	VII	
ET_p	Significant increase	3	5	2	2	8	25	5	50
	Insignificant increase	23	24	19	36	55	117	29	303
	No trend	0	0	0	0	0	4	0	4
	Insignificant decrease	20	15	16	28	41	43	18	181
	Significant decrease	0	3	2	3	4	1	0	13
ET_0	Significant increase	0	1	0	2	5	14	3	25
	Insignificant increase	17	16	9	24	34	60	16	176
	No trend	0	0	0	0	1	4	0	5
	Insignificant decrease	27	27	25	36	60	100	30	305
	Significant decrease	2	3	5	7	8	12	3	40

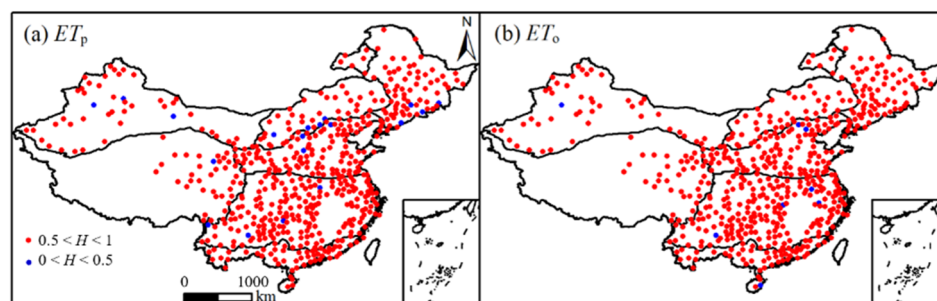


Figure 10. The spatial distribution of the Hurst index denoting the long-term dependence of ET_p and ET_0 .

Table 3. The station numbers of the Hurst coefficient for annual ET_0 and ET_p in different sub-regions.

Sub-Region		I	II	III	IV	V	VI	VII	Subtotal
ET_p	$0.5 < H < 1$	43	43	38	65	105	186	52	532
	$0 < H < 0.5$	3	4	1	4	3	4	0	19
ET_0	$0.5 < H < 1$	45	47	39	69	106	186	51	543
	$0 < H < 0.5$	1	0	0	0	2	4	1	8

3.2.3. The Wavelet Periods

The variations in the wavelet spectrum and the wavelet variance for the annual ET_p and ET_0 between 1961 and 2018 in mainland China are presented in Figure 11. The vibration intensity and fluctuation characteristics of the annual ET_p and ET_0 were very similar. The primary and secondary periods of the annual ET_p and ET_0 were almost same, being about 10 and 2 years, respectively, though somewhat weak. This was reasonable, since their annual variation patterns were very similar, although their values were very different (see Figure 7). Among the different time intervals, there were significant periods of four years between 1961 and 1970.

The spatial distributions of the primary periods in the annual ET_p and ET_0 for all the studied sites are mapped and presented in Figure 12. In general, sites with shorter periods and with longer periods have similar distribution characteristics for both the annual ET_p and ET_0 . They were mainly distributed in sub-regions V-VII, while a few were distributed in the other sub-regions.

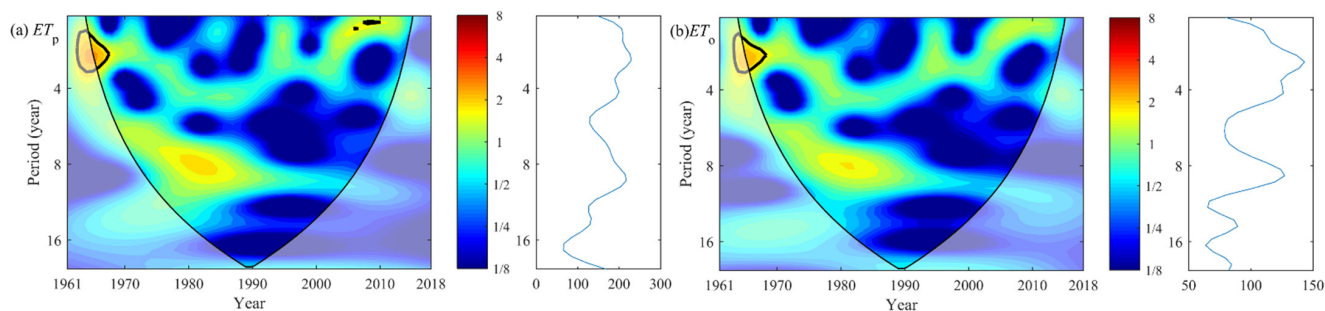


Figure 11. The wavelet spectrum and wavelet variance for the annual ET_p (a) and ET_o (b) of mainland China. The thin solid lines denote the cones of influence, and the thick solid lines show the 95% confidence levels. The color bar represents the vibration intensity of the periods at different timescales.

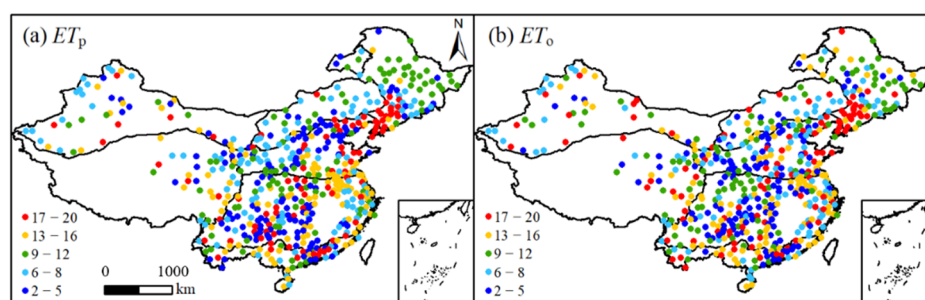


Figure 12. The main periods of annual ET_p (a) and ET_o (b) extracted from wavelet analysis.

4. Discussion

Though differentiating ET_p and ET_o seems easy, it is in fact very difficult and can greatly impact their further application. The standard method of the FAO-56 PM equation for ET_o [6] has been universally accepted. However, no standard method for the ET_p has been proposed. This research takes the Penman (1963) equation as the standard method for ET_p , considering it is a combination-type equation and has generally good performance [25]. Moreover, several pieces of research found that the value of ET_p was higher than that of ET_o on a daily scale; for example, the root mean square errors between ET_p and ET_o were 1.88 mm/d and 0.93 mm/d in the Senegal River Valley and North China Plain, respectively [69,70]. These research specialized the wind effects and the dynamic process of vaporization by adding specific numbers to represent the study area. However, this is still not a universal method. The Thornthwaite (1948) equation is also used to calculate ET_p , requiring only temperature data [23]. However, it tends to underestimate ET_p in humid regions [71,72]. There may be other better ET_p equations used in different countries. Nevertheless, there are apparent differences, especially in the spatiotemporal variations, between the ET_p and ET_o , at monthly, annual, and other timescales.

Since the monthly and annual values, ranges, seasonal changes, spatial distributions, long-term dependent characteristics, periods, trends, and significance of ET_p and ET_o differed at most of the sites in the sub-regions and in mainland China, in the future the unitization of the two terms should be approached more carefully. Not only do the quantitative characteristics of ET_p and ET_o differ, but the application scale differs as well. ET_p has been suitably applied to studies with a larger spatial scale, including the rainfall-runoff modeling of many catchments [39], discharge projections [73], and the attribution of evapotranspiration changes under non-water-limited conditions [15], as well as drought severity analysis on a regional, national and global scale [74–76]. Comparatively, ET_o is applied on smaller spatial scales, including site, field, and regional scales [43,44,46,47,49].

In addition, there was variability in the D series on the monthly and yearly timescales, as clearly shown by Anselin Local Moran's I index [77] (Table 4, Figures S1 and S2). More studies are needed for detailed descriptions. It is easy to see that the major Moran's type of

D series is not significant, that there is a high proportion of High-High (HH) or Low-Low (LL) clusters in the rest sites, and that there are only a few sites representing the High-Low (HL) or Low-High (LH) outlier. The Moran's type spatial distribution of monthly and yearly D also depicted a similar annual trend showing that the HH or LL sites' position will reverse to each other in a year (Figures S1 and S2).

Table 4. The site numbers of Anselin Local Moran's I index for D series.

Timesclae Moran's I	Monthly												Yearly
	January	February	March	April	May	June	July	August	September	October	November	December	
NS	338	370	342	337	328	285	406	435	407	391	367	341	383
HH	97	78	96	95	88	102	63	48	61	67	76	89	79
HL	0	1	3	4	4	3	3	3	2	3	1	1	3
LH	2	4	7	8	7	6	6	5	6	5	5	3	7
LL	114	98	103	107	124	155	73	60	75	85	102	117	79

Notes: NS: not significant; HH: High-High Cluster; HL: High-Low Outlier; LH: Low-High Outlier; LL: Low-Low Cluster.

5. Conclusions

The differences between ET_p and ET_o at monthly and annual timescales in China were studied between 1961 and 2018. At most sites in most months, the ET_p was larger than the ET_o . Except for some similarity in the long-term dependence indicated by the Hurst index and the spatial distribution of the primary period calculated by wavelet analysis, generally there were many differences between the ET_p and ET_o .

At different timescales, ET_p and ET_o showed some similar situations and some different behaviors. Their values were closer in some months than in others because of the lower influence of the surface resistance of evapotranspiration in the calculation equations. Different spatial distributions in various sub-regions and mainland China were found. These were related to the variation in weather data under different situations. As for the monthly ET_p and ET_o , at most of the sites in every sub-region, the ET_p was higher than the ET_o . This result provides supportive guidance for the related policy managers to deal with water risk management. The maximum difference was observed in May or July, and the minimum difference was observed in December or January. Different distribution trends of ET_p and ET_o were also shown. On the annual scale, the ET_p and ET_o showed a similar spatial distribution but different quantities, and there was an obvious difference in the significance, future trend, and primary periods at all stations. This confirmed the discrepancy of the spatial-temporal variations between ET_p and ET_o . Overall, our results strongly indicate that researchers should use ET_p and ET_o carefully and be sure to differentiate them.

Supplementary Materials: The following supporting information can be downloaded at: <https://www.mdpi.com/article/10.3390/w14060988/s1>, Figure S1: The Anselin Local Moran's I index distribution of monthly D; Figure S2: The Anselin Local Moran's I index distribution of yearly ET_p , ET_o and D respectively.

Author Contributions: Conceptualization, K.X., X.Z. and Y.L.; Methodology, K.X.; Software, K.X.; Validation, X.P. and N.Y.; Original draft preparation writing, K.X. and Y.L.; Review and Editing, A.B., D.L.L., F.L., Y.Z., B.P. and F.L. All authors have read and agreed to the published version of the manuscript.

Funding: This research was funded by National Key Research and Development Program of China (2019YFA0606902), the Science and Technology Project of Tumushuk, Third Division (No. S202102GG018); and the National Natural Science Foundation of China (No. 52079114).

Informed Consent Statement: Informed consent was obtained from all subjects involved in the study.

Data Availability Statement: The weather data can be found from China Meteorological Data Sharing center (<http://data.cma.cn/> (accessed on 8 February 2022)).

Conflicts of Interest: The authors declare no conflict of interest.

Abbreviations

ET_p —potential evapotranspiration; ET_o —reference crop evapotranspiration; R^2 —coefficient of determination; FAO—Food and Agriculture Organization; R/S—rescaled; MMK—modified Mann–Kendall.

References

- Milly, P.C.D.; Dunne, K.A. Potential evapotranspiration and continental drying. *Nat. Clim. Change* **2016**, *6*, 946–949. [[CrossRef](#)]
- Peng, L.; Li, Y.; Feng, H. The best alternative for estimating reference crop evapotranspiration in different sub-regions of mainland China. *Sci. Rep.* **2017**, *7*, 5458. [[CrossRef](#)] [[PubMed](#)]
- Vörösmarty, C.J.; Federer, C.A.; Schloss, A.L. Potential evaporation functions compared on US watersheds: Possible implications for global-scale water balance and terrestrial ecosystem modeling. *J. Hydrol.* **1998**, *207*, 147–169. [[CrossRef](#)]
- Yao, N.; Li, Y.; Dong, Q.G.; Li, L.; Peng, L.; Feng, H. Influence of the accuracy of reference crop evapotranspiration on drought monitoring using standardized precipitation evapotranspiration index in mainland China. *Land. Degrad. Dev.* **2020**, *31*, 266–282. [[CrossRef](#)]
- Zhang, Y. Estimation of Potential Evapotranspiration by Different Methods in Handan Eastern Plain, China. *Water Sci. Eng.* **2019**, *4*, 117.
- Allen, R.G.; Pereira, L.S.; Raes, D.; Smith, M. Crop evapotranspiration: Guidelines for computing crop water requirements. In *Irrigation and Drainage Paper No 56*; Food and Agriculture Organization of the United Nations (FAO): Rome, Italy, 1998.
- Ohana-Levi, N.; Ben-Gal, A.; Munitz, S.; Netzer, Y. Grapevine crop evapotranspiration and crop coefficient forecasting using linear and non-linear multiple regression models. *Agric. Water Manag.* **2022**, *262*, 107317. [[CrossRef](#)]
- Hu, K.; Awange, J.; Kuhn, M.; Zerihun, A. Irrigated agriculture potential of Australia’s northern territory inferred from spatial assessment of groundwater availability and crop evapotranspiration. *Agric. Water Manag.* **2022**, *264*, 107466. [[CrossRef](#)]
- Gentilucci, M.; Barbieri, M.; Burt, P. (Eds.) Climate and territorial suitability for the Vineyards developed using GIS techniques. In Proceedings of the Conference of the Arabian Journal of Geosciences, Sousse, Tunisia, 2–5 November 2018.
- Saadi, S.; Todorovic, M.; Tanasijevic, L.; Pereira, L.S.; Pizzigalli, C.; Lionello, P. Climate change and Mediterranean agriculture: Impacts on winter wheat and tomato crop evapotranspiration, irrigation requirements and yield. *Agric. Water Manag.* **2015**, *147*, 103–115. [[CrossRef](#)]
- Fan, J.; Wu, L.; Zhang, F.; Xiang, Y.; Zheng, J. Climate change effects on reference crop evapotranspiration across different climatic zones of China during 1956–2015. *J. Hydrol.* **2016**, *542*, 923–937. [[CrossRef](#)]
- Saray, M.H.; Eslamian, S.S.; Klove, B.; Gohari, A. Regionalization of potential evapotranspiration using a modified region of influence. *Theor. Appl. Climatol.* **2019**, *140*, 115–127. [[CrossRef](#)]
- Silva, C.R.D.; Barbosa, L.A.; Finzi, R.R.; Riberio, B.T.; Dias, N.D.S. Accuracy of air temperature forecasts and its use for prediction of the reference evapotranspiration. *Biosci. J.* **2020**, *36*, 17–22. [[CrossRef](#)]
- Um, M.; Kim, Y.; Park, D.; Jung, K.; Wang, Z.; Kim, M.M.; Shin, H. Impacts of potential evapotranspiration on drought phenomena in different regions and climate zones. *Sci. Total Environ.* **2020**, *703*, 135590. [[CrossRef](#)] [[PubMed](#)]
- Yang, Y.; Roderick, M.L.; Zhang, S.; Mcvicar, T.R.; Donohue, R.J. Hydrologic implications of vegetation response to elevated CO₂ in climate projections. *Nat. Clim. Change* **2019**, *9*, 44–48. [[CrossRef](#)]
- Li, J.; Wu, C.; Wang, X.; Peng, J.; Dong, D.; Lin, G.; Gonsamo, A. Satellite observed indicators of the maximum plant growth potential and their responses to drought over Tibetan Plateau (1982–2015). *Ecol. Indic.* **2020**, *108*, 105732. [[CrossRef](#)]
- Zhao, J.; Wang, Z. Future trends of water resources and influences on agriculture in China. *PLoS ONE* **2020**, *15*, e0231671. [[CrossRef](#)]
- Shanmugam, M.; Mekonnen, M.; Ray, C. Grid-Based Model for Estimating Evapotranspiration Rates of Heterogeneous Land Surface. *J. Irrig. Drain. Eng.* **2020**, *146*, 04019030. [[CrossRef](#)]
- Malik, A.; Kumar, A.; Ghorbani, M.A.; Kashani, M.H.; Kisi, O.; Kim, S. The viability of co-active fuzzy inference system model for monthly reference evapotranspiration estimation: Case study of Uttarakhand State. *Hydrol. Res.* **2019**, *50*, 1623–1644. [[CrossRef](#)]
- You, G.; Arain, M.A.; Wang, S.; Lin, N.; Wu, D.; McKenzie, S.; Zou, C.; Liu, B.; Zhang, X.; Gao, J. Trends of actual and potential evapotranspiration based on Bouchet’s complementary concept in a cold and arid steppe site of Northeastern Asia. *Agr. For. Meteorol.* **2019**, *279*, 107684. [[CrossRef](#)]
- Adhikari, A.; Mainali, K.P.; Rangwala, I.; Hansen, A.J. Various measures of potential evapotranspiration have species-specific impact on species distribution models. *Ecol. Model.* **2019**, *414*, 108836. [[CrossRef](#)]
- Guo, D.; Westra, S.; Maier, H.R. An R package for modelling actual, potential and reference evapotranspiration. *Environ. Model. Softw.* **2016**, *78*, 216–224. [[CrossRef](#)]
- Thorntwaite, C.W. An Approach toward a Rational Classification of Climate. *Geogr. Rev.* **1948**, *38*, 55–94. [[CrossRef](#)]
- Penman, H.L. Evaporation: An introductory survey. *Neth. J. Agri. Sci.* **1956**, *4*, 9–29. [[CrossRef](#)]
- Penman, H.L. (Ed.) *Vegetation and Hydrology, Tech. Commun. 53*, Commonwealth Bureau of Soils; Soil Science: Harpenden, UK, 1963.
- Anon, J. Proceeding of the informal meeting on physics in agriculture. *Neth. J. Agri. Sci.* **1956**, *4*, 162–175.

27. WMO. *Sites for Wind-Power Installations*; WMO No. 156, Technical Note No. 63; WMO: Geneva, Switzerland, 1963. Available online: https://library.wmo.int/index.php?lvl=notice_display&id=5475#.YjfmEHpBzDc (accessed on 8 February 2022).
28. Jensen, M.E. Water Consumption by Agricultural Plants. In *Plant Water Consumption & Response. Volume II. Water Deficits and Plant Growth*; Kozłowski, T.T., Ed.; Academic Press: New York, NY, USA; London, UK, 1968; pp. 1–22.
29. Granger, R.J. An examination of the concept of potential evaporation. *J. Hydrol.* **1989**, *111*, 9–19. [[CrossRef](#)]
30. Doorenbos, J.; Pruitt, W. *Guidelines for Predicting Crop Water Requirements, Irrigation and Drainage Paper No. 24*; FAO: Rome, Italy, 1977.
31. Ochoa-Sánchez, A.; Crespo, P.; Carrillo-Rojas, G.; Sucozhañay, A.; Célleri, R. Actual Evapotranspiration in the High Andean Grasslands: A Comparison of Measurement and Estimation Methods. *Front. Earth Sci.* **2019**, *7*, 55. [[CrossRef](#)]
32. Chen, S.; Liu, Y.; Axel, T. Climatic change on the Tibetan Plateau: Potential Evapotranspiration Trends from 1961–2000. *Clim. Change* **2006**, *76*, 291–319.
33. Seiller, G.; Anctil, F. How do potential evapotranspiration formulas influence hydrological projections? *Hydrolog. Sci. J.* **2016**, *61*, 2249–2266. [[CrossRef](#)]
34. Sun, C.; Zheng, Z.; Chen, W.; Wang, Y. Spatial and Temporal Variations of Potential Evapotranspiration in the Loess Plateau of China during 1960–2017. *Sustainability* **2020**, *12*, 354. [[CrossRef](#)]
35. Sun, S.; Lei, S.; Jia, H.; Li, C.; Zhang, J.; Meng, P. Tree-Ring Analysis Reveals Density-Dependent Vulnerability to Drought in Planted Mongolian Pines. *Forests* **2020**, *11*, 98. [[CrossRef](#)]
36. Gwate, O.; Mantel, S.K.; Palmer, A.R.; Gibson, L.; Munch, Z. Measuring and modelling evapotranspiration in a South African grassland: Comparison of two improved Penman-Monteith formulations. *Water SA* **2018**, *44*, 482–494. [[CrossRef](#)]
37. Lewis, C.S.; Allen, L.N. Potential Crop Evapotranspiration and Surface Evaporation Estimates via a Gridded Weather Forcing Dataset. *J. Hydrol.* **2017**, *546*, 450–463. [[CrossRef](#)]
38. Ding, H.; Xingming, H.; Ying, H.; Jingxiu, Q. Uncertainty assessment of potential evapotranspiration in arid areas, as estimated by the Penman-Monteith method. *J. Arid. Land* **2020**, *12*, 166–180.
39. Oudin, L.; Hervieu, F.; Michel, C.; Perrin, C.; Andreassian, V.; Anctil, F.; Loumagne, C. Which potential evapotranspiration input for a lumped rainfall-runoff model? Part 2: Towards a simple and efficient potential evapotranspiration model for rainfall-runoff modelling. *J. Hydrol.* **2005**, *303*, 290–306. [[CrossRef](#)]
40. Jensen, M.E.; Burman, R.D.; Allen, R.G. *Evapotranspiration and Irrigation Water Requirements*; Agriculture Society Civil Engineering: New York, NY, USA, 1990.
41. Hargreaves, G.H.; Samani, Z.A. Estimating potential evapotranspiration. *J. Irrig. Drain. Div.* **1982**, *108*, 225–230. [[CrossRef](#)]
42. Hargreaves, G.H.; Samani, Z.A. Reference crop evapotranspiration from temperature. *Appl. Eng. Agric.* **1985**, *1*, 96–99. [[CrossRef](#)]
43. Dinpashoh, Y.; Jhajharia, D.; Fakheri-Fard, A.; Singh, V.P.; Kahya, E. Trends in reference crop evapotranspiration over Iran. *J. Hydrol.* **2011**, *399*, 422–433. [[CrossRef](#)]
44. Feng, Y.; Cui, N.; Zhao, L.; Hu, X.; Gong, D. Comparison of ELM, GANN, WNN and empirical models for estimating reference evapotranspiration in humid region of Southwest China. *J. Hydrol.* **2016**, *536*, 376–383. [[CrossRef](#)]
45. Gong, L.; Xu, C.; Chen, D.; Halldin, S.; Chen, Y.D. Sensitivity of the Penman–Monteith reference evapotranspiration to key climatic variables in the Changjiang (Yangtze River) basin. *J. Hydrol.* **2006**, *329*, 620–629. [[CrossRef](#)]
46. Hargreaves, G.H.; Allen, R.G. History and evaluation of Hargreaves evapotranspiration equation. *J. Irrig. Drain. Eng.* **2003**, *129*, 53–63. [[CrossRef](#)]
47. Li, Z.; Zheng, F.; Liu, W. Spatiotemporal characteristics of reference evapotranspiration during 1961–2009 and its projected changes during 2011–2099 on the Loess Plateau of China. *Agr. For. Meteorol.* **2012**, *154*, 147–155. [[CrossRef](#)]
48. Mcvicar, T.R.; Van Niel, T.G.; Li, L.; Hutchinson, M.F.; Mu, X.; Liu, Z. Spatially distributing monthly reference evapotranspiration and pan evaporation considering topographic influences. *J. Hydrol.* **2007**, *338*, 196–220. [[CrossRef](#)]
49. Tabari, H.; Marofi, S.; Aeini, A.; Talaei, P.H.; Mohammadi, K. Trend analysis of reference evapotranspiration in the western half of Iran. *Agr. For. Meteorol.* **2011**, *151*, 128–136. [[CrossRef](#)]
50. Chattopadhyay, N.; Hulme, M. Evaporation and potential evapotranspiration in India under conditions of recent and future climate change. *Agr. For. Meteorol.* **1997**, *87*, 55–73. [[CrossRef](#)]
51. Han, S.; Xu, D.; Wang, S. Decreasing potential evaporation trends in China from 1956 to 2005: Accelerated in regions with significant agricultural influence? *Agr. For. Meteorol.* **2012**, *154*, 44–56. [[CrossRef](#)]
52. Wang, K.; Xu, Q.; Li, T. Does recent climate warming drive spatiotemporal shifts in functioning of high-elevation hydrological systems? *Sci. Total Environ.* **2020**, *719*, 137507. [[CrossRef](#)]
53. Katerji, N.; Rana, G. Crop reference evapotranspiration: A discussion of the concept, analysis of the process and validation. *Water Resour. Manag.* **2011**, *25*, 1581–1600. [[CrossRef](#)]
54. Xiang, K.; Li, Y.; Horton, R.; Feng, H. Similarity and difference of potential evapotranspiration and reference crop evapotranspiration - a review. *Agric. Water Manag.* **2020**, *232*, 106043. [[CrossRef](#)]
55. Helsel, D.R.; Hirsch, R.M. *Statistical Methods in Water Resources*; Elsevier: Amsterdam, The Netherlands, 1992.
56. Ayantobo, O.O.; Li, Y.; Song, S.; Yao, N. Spatial comparability of drought characteristics and related return periods in mainland China over 1961–2013. *J. Hydrol.* **2017**, *550*, 549–567. [[CrossRef](#)]
57. Yao, N.; Li, Y.; Lei, T.; Peng, L. Drought evolution, severity and trends in mainland China over 1961–2013. *Sci. Total Environ.* **2018**, *616*, 73–89. [[CrossRef](#)]

58. Li, S.; Kang, S.; Zhang, L.; Zhang, J.; Du, T.; Tong, L.; Ding, R. Evaluation of six potential evapotranspiration models for estimating crop potential and actual evapotranspiration in arid regions. *J. Hydrol.* **2016**, *543*, 450–461. [[CrossRef](#)]
59. Xu, K.; Yang, D.; Yang, H.; Li, Z.; Qin, Y.; Shen, Y. Spatio-temporal variation of drought in China during 1961–2012: A climatic perspective. *J. Hydrol.* **2015**, *526*, 253–264. [[CrossRef](#)]
60. Yang, Y.; Chen, R.; Song, Y.; Han, C.; Liu, J.; Liu, Z. Sensitivity of potential evapotranspiration to meteorological factors and their elevational gradients in the Qilian Mountains, northwestern China. *J. Hydrol.* **2019**, *568*, 147–159. [[CrossRef](#)]
61. Yue, S.; Wang, C.Y. Regional Streamflow Trend Detection with Consideration of Both Temporal and Spatial Correlation. *Int. J. Climatol.* **2002**, *22*, 933–946. [[CrossRef](#)]
62. Mann, H.B. Nonparametric Tests against Trend. *Econometrica* **1945**, *13*, 245–259. [[CrossRef](#)]
63. Kendall, M.G. Rank Auto Correlation Methods. *Brit. J. Psychol.* **1976**, *25*, 86–97.
64. Li, Y.; Horton, R.; Ren, T.; Chen, C. Prediction of annual reference evapotranspiration using climatic data. *Agric. Water Manag.* **2010**, *97*, 300–308. [[CrossRef](#)]
65. Mandelbrot, B.B.; Wallis, J.R. Robustness of the rescaled range R/S in the measurement of noncyclic long run statistical dependence. *Water Resour. Res.* **1969**, *5*, 967–988. [[CrossRef](#)]
66. Hurst, H.E. Long-term storage capacity of reservoirs. *Trans. Am. Soc. Civil. Eng.* **1951**, *116*, 770–808. [[CrossRef](#)]
67. Liu, Y.; Li, Y.; Li, L.; Chen, C. Spatiotemporal Variability of Monthly and Annual Snow Depths in Xinjiang, China over 1961–2015 and the Potential Effects. *Water* **2019**, *11*, 1666. [[CrossRef](#)]
68. Li, L.; Yao, N.; Li, Y.; Liu, D.L.; Wang, B.; Ayantobo, O.O. Future projections of extreme temperature events in different sub-regions of China. *Atmos. Res.* **2019**, *217*, 150–164. [[CrossRef](#)]
69. Djaman, K.; Balde, A.B.; Sow, A.; Muller, B.; Irmak, S.; N'Diaye, M.K.; Manneh, B.; Moukoumbi, Y.D.; Futakuchi, K.; Saito, K. Evaluation of sixteen reference evapotranspiration methods under sahelian conditions in the Senegal River Valley. *J. Hydrol.* **2015**, *3*, 139–159. [[CrossRef](#)]
70. Liu, X.; Xu, C.; Zhong, X.; Li, Y.; Yuan, X.; Cao, J. Comparison of 16 models for reference crop evapotranspiration against weighing lysimeter measurement. *Agric. Water Manag.* **2017**, *184*, 145–155. [[CrossRef](#)]
71. Sentelhas, P.C.; Gillespie, T.J.; Santos, E.A. Evaluation of FAO Penman–Monteith and alternative methods for estimating reference evapotranspiration with missing data in Southern Ontario, Canada. *Agric. Water Manag.* **2010**, *97*, 635–644. [[CrossRef](#)]
72. Valipour, M.; Sefidkouhi, M.A.G.; Raeini, M. Selecting the best model to estimate potential evapotranspiration with respect to climate change and magnitudes of extreme events. *Agric. Water Manag.* **2017**, *180*, 50–60. [[CrossRef](#)]
73. Dakhlaoui, H.; Seibert, J.; Hakala, K. Sensitivity of discharge projections to potential evapotranspiration estimation in Northern Tunisia. *Reg. Environ. Change* **2020**, *20*, 34. [[CrossRef](#)]
74. Burke, E.J.; Brown, S.I.J.; Christidis, N. Modeling the Recent Evolution of Global Drought and Projections for the Twenty-First Century with the Hadley Centre Climate Model. *J. Hydrometeorol.* **2006**, *7*, 1113–1125. [[CrossRef](#)]
75. Li, Y.; Sun, C. Impacts of the superimposed climate trends on droughts over 1961–2013 in Xinjiang, China. *Theor. Appl. Climatol.* **2017**, *129*, 977–994. [[CrossRef](#)]
76. Yao, N.; Li, L.; Feng, P.; Feng, H.; Liu, D.L.; Liu, Y.; Jiang, K.; Hu, X.; Li, Y. Projections of drought characteristics in China based on a standardized precipitation and evapotranspiration index and multiple GCMs. *Sci. Total Environ.* **2020**, *704*, 135245. [[CrossRef](#)]
77. Anselin, L. Local indicators of spatial association—LISA. *Geogr. Anal.* **1995**, *27*, 93–115. [[CrossRef](#)]